Scilight

Nanoenergy Communications

https://www.sciltp.com/journals/nc

Review

Check for updates

Droplet Electricity Harvesting: From Liquid-Solid Interface to Energy-per-Droplet

Pawantree Promsuwan [1,2] and Ya Yang [1,2,*]

[1] Beijing Key Laboratory of Micro-Nano Energy and Sensor, Center for High-Entropy Energy and Systems, Beijing Institute of Nanoenergy and Nanosystems, Chinese Academy of Sciences, Beijing 101400, China
[2] School of Nanoscience and Engineering, University of Chinese Academy of Sciences, Beijing 100049, China
* Correspondence: yayang@binn.cas.cn

How To Cite: Promsuwan, P.; Yang, Y. Droplet Electricity Harvesting: From Liquid-Solid Interface to Energy-per-Droplet. *Nanoenergy Communications* **2026**, *1*(1), 7. https://doi.org/10.53941/nc.2026.100007

Received: 2 April 2026
Revised: 27 April 2026
Accepted: 30 April 2026
Published: 9 May 2026

Abstract: The growing demand for energy, along with the environmental and economic challenges associated with fossil fuel consumption, has created an urgent need for renewable energy sources. Water-based sources are considered a potential source of renewable energy because about 71% of the Earth's surface is covered by water. With advances in droplet-based triboelectric nanogenerators and droplet electricity generators, and the ubiquity of water, energy harvesting using droplet-based systems has become a promising method for capturing ambient mechanical energy with straightforward device designs. To better understand droplet electricity harvesting, this review summarizes the fundamental mechanisms of droplet-induced electricity generation, discusses the performance metrics needed for reliable device comparison, and highlights major strategies for improving output and efficiency. Representative applications of these systems and assess the principal challenges that currently limit their practical implementation are further examined. By elucidating the connections among mechanisms, performance, and applications, this review provides a framework for the continued advancement of droplet-based electricity-harvesting technologies.

Keywords: droplet-based TENGs; droplet electricity generators; metrics for device performance comparison; droplet energy harvesting

1. Introduction

The shift away from fossil fuels is urgent due to rising pollution, climate change, dwindling reserves, and volatile oil prices [1]. Accordingly, renewable energy sources, including solar, wind, and water-based sources such as raindrops, streams, rivers, reservoirs, and the ocean, are gaining interest for their lower environmental impact. Furthermore, locally generated renewable energy provides advantages beyond emissions reduction. By decentralizing power generation, these systems can lessen dependence on imported fossil fuels and enhance energy security, enhance resilience to climatic and geopolitical shocks, safeguard essential services during emergencies, and cushion communities and national economies against supply disruptions and price volatility [2].

Water-based renewable resources represent a vast and widely distributed energy reservoir, as water covers 71% of the Earth's surface [3]. Sources that can be harnessed for electricity generation include oceans, reservoirs, rivers, waterfalls, raindrops, and atmospheric water, such as mist and fog [4–7], as shown in Figure 1. Considerable efforts have long been devoted to exploiting these resources, with electromagnetic generators serving as the dominant technology for large-scale water-energy harvesting from systems such as rivers, dams, and steam-driven turbines. However, these approaches are poorly suited to dispersed, small-volume water sources. The emergence of liquid-solid triboelectric nanogenerators (TENGs) in 2014 [8] opened a new route for harvesting energy from droplets and other microscale forms of water. In recent years, numerous review articles have summarized and

discussed the mechanisms governing droplet-TENGs (D-TENGs) and droplet electricity generators (DEGs), and have illustrated their broad potential for practical applications [9–13].

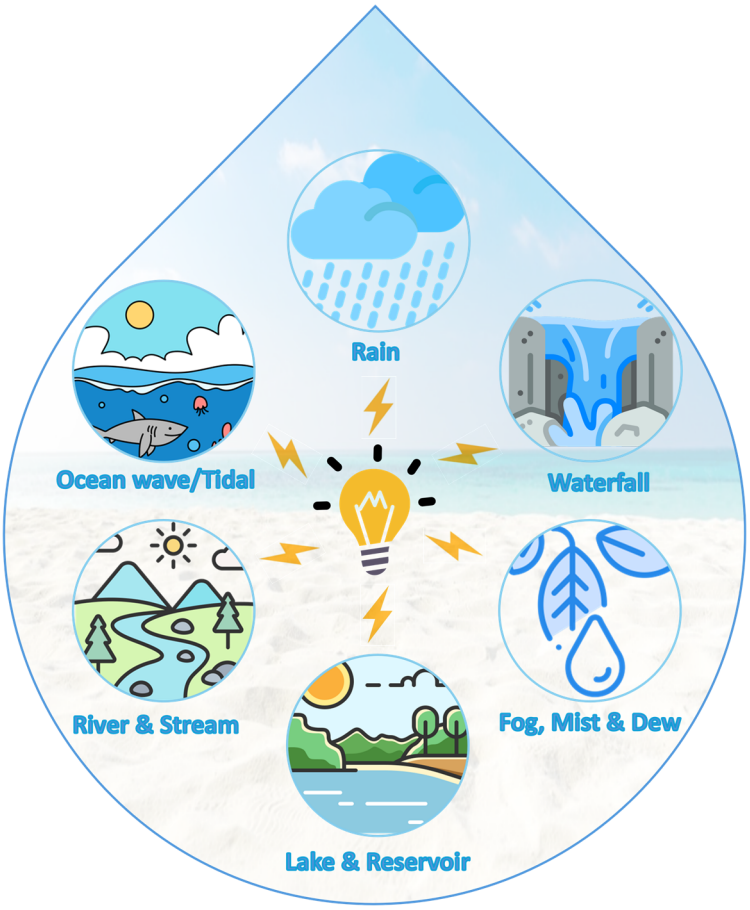

Figure 1. Water-based renewable resources for electricity generation. (Icons are downloaded from www.freepik.com [14]).

In this review, the fundamental mechanisms governing droplet-based triboelectric nanogenerators are summarized. Importantly, criteria for comparing the efficiency of devices fabricated and tested under different conditions are introduced to ensure that the energy generated by a single droplet accurately reflects intrinsic device performance. Strategically, several routes to enhancing device efficiency are highlighted, including exploring new mechanisms, developing new device architectures, and tuning material properties. Finally, the key challenges and future directions in D-TENGs and DEGs are highlighted, providing insights to improve mechanisms, device design, performance, and practical applications in droplet energy harvesting. Overall, this review provides a framework for the continued advancement of droplet-based electricity-harvesting technologies by elucidating the connections among mechanisms, performance, and applications.

2. The Properties of Static and Dynamic Droplets

2.1. Static Droplet Properties

In D-TENGs and DEGs, the liquid-solid interface is key to understanding the mechanisms that underlie these devices, as elucidating them helps improve their performance. In the static state, when a liquid droplet contacts a solid substrate, it spreads to lower the system's free energy and eventually settles into a minimum-energy state [15], determining the droplet's equilibrium shape. In equilibrium, the droplet shape depends on the interfacial tensions (Figure 2a) that are explained through Young's equation, $\cos\theta = \frac{\gamma_{SV}-\gamma_{SL}}{\gamma_{LV}}$, where the contact angle in equilibrium that the droplet makes with a solid surface is represented by θ and γ_{SV}, γ_{SL}, and γ_{LV} are solid-vapor, solid-liquid, and liquid-vapor interfacial tensions, respectively [16]. The behavior of droplets on the surface can be categorized by the contact angle (θ), whether it is superhydrophilic, hydrophilic, hydrophobic, or superhydrophobic when $0° < \theta < 10°$, $10° < \theta < 90°$, $90° < \theta < 150°$, and $150° < \theta < 180°$, respectively [17,18].

The contact angle characterized by Young's equation is based on a stationary condition with a flat and smooth surface, while a contact angle hysteresis ($\Delta\theta$) is measured through the dynamic droplet-interface motion

experiments, and considered when the surface is heterogeneous. Surface heterogeneity can cause the advancing contact angle (θ_A) and the receding contact angle (θ_R) [15]. The contact angle hysteresis (Figure 2b) refers to the variation between the advancing contact angle and receding contact angle ($\Delta\theta = \theta_A - \theta_R$). These dynamic tests of droplets on a surface are performed by inclining a flat substrate to a defined angle, termed the sliding angle (α). To achieve superhydrophobic surfaces, it is essential to have a greater contact angle and smaller hysteresis for water droplets to rebound and roll off.

Superhydrophobic surfaces exhibit strong water repellency and droplet motion due to their high contact angles and minimal contact angle hysteresis. This occurs since gas pockets are confined at the liquid-solid interface, leading to the Cassie-Baxter state (Figure 2c (left image)). Conversely, the Wenzel state (Figure 2c (right image)) encompasses full wetting by the liquid. These states can shift from one to another due to pressure changes during droplet evaporation, even in static conditions [19].

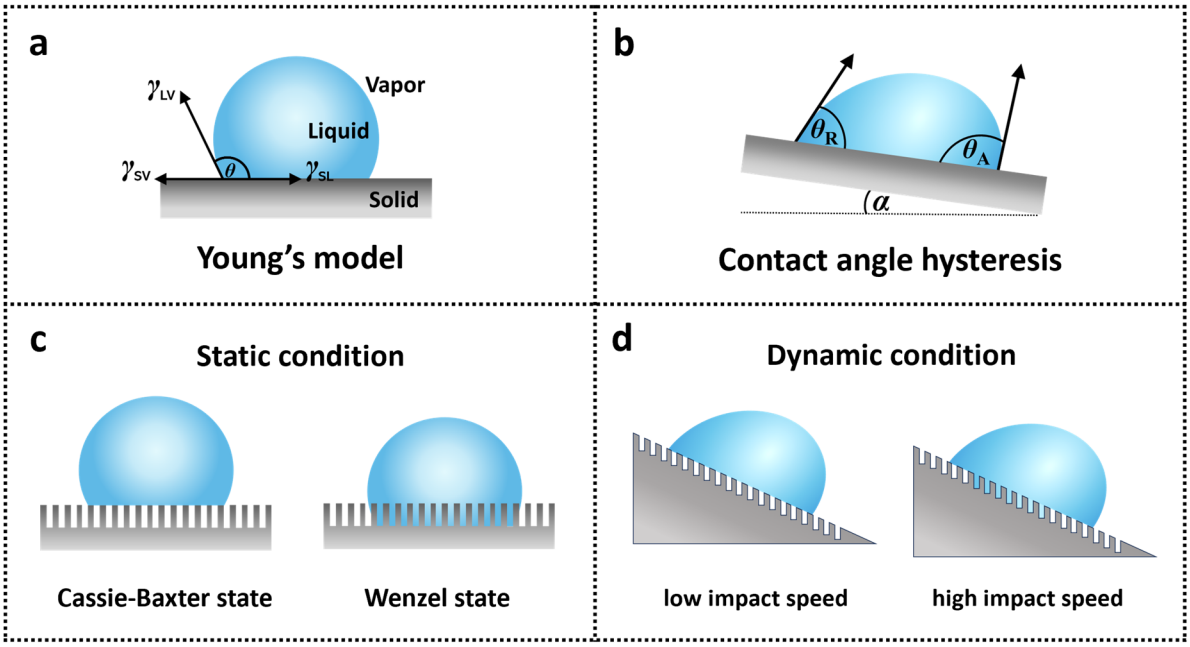

Figure 2. The droplet behavior in static and dynamic conditions. (**a**) The droplet shape on a solid substrate in equilibrium. (**b**) The contact angle hysteresis. (**c**) Cassie-Baxter state (left) and Wenzel state (right). (**d**) Preservation of the Cassie-Baxter state at low droplet impact velocities (left) and local-impalement-driven suppression of droplet rebound above a surface-dependent critical impact velocity (right).

2.2. Dynamic Droplet Properties

Dynamic droplet properties are crucial to governing the operating mechanism of droplet electricity devices. When a droplet impacts a surface, it deforms in ways such as spreading, rebounding, and detaching, which influences the devices' output performance. When the droplet impacts the surface at low speeds, the Cassie-Baxter state can be maintained (Figure 2d (left image)), allowing the drop to rebound. Once the impact velocity exceeds a surface-dependent threshold, local impalement can suppress droplet rebound by driving a Cassie-Baxter-to-Wenzel wetting transition (Figure 2d (right image)) [19].

Antonini et al. [19] systematically analyzed the kinematics of oblique droplet impact on inclined hydrophobic and superhydrophobic surfaces. Their finding indicates that surface tilt and wettability can directly regulate contact time, contact-line speed, and droplet removal [19], all of which are key electrical variables in D-TENGs and DEGs. Recently, Srivastava et al. [20] experimentally investigated how water droplets spread on inclined surfaces with varying wettability and revealed that spreading occurs in three distinct stages: an initial regime driven by inertia, a middle stage of asymmetric spreading characterized by maximum lateral extent, and a final stage in which gravity assists downstream elongation. They also found that the normal Weber number primarily governs the maximum lateral spread, while gravity increasingly influences the subsequent longitudinal extension, especially at steeper angles and on more wet surfaces. By demonstrating how inclination-induced asymmetry, lamella pinning, and gravity-aided elongation influence droplet contact dynamics, this study provides useful hydrodynamic insight that may inform the design of droplet-TENGs and DEGs.

3. Mechanisms Governing Droplet Electricity Harvesting

Understanding the mechanisms underlying electricity generation in each device structure informs structural design, materials engineering, and material selection, thereby improving device performance.

3.1. Contact Electrification and Electrostatic Induction

The mechanistic foundations of most D-TENGs are contact electrification (CE) and electrostatic induction (EI). The integration of triboelectric theory with the electrical double layer (EDL) is the main mechanism of CE and EI [21]. CE at the interface between liquid and solid is the charge distribution induced when a liquid droplet touches a solid surface. Quantitative analysis indicates that both electrons and ions are transferred upon contact, with electrons being the major transferred species [22].

According to the first D-TENG pioneered by Wang and his team, the device is a single-electrode mode D-TENG [8]. The droplet carries triboelectric charge, which can be negative or positive depending on the surface it contacts, due to friction with air, pipes, or a polytetrafluoroethylene (PTFE) surface. A positive voltage develops between the copper electrode (Cu) and the ground when a positively charged water droplet approaches the PTFE film. In the short-circuit configuration, from the ground to the Cu, electrons flow in response to the potential difference until the system reaches balance, thereby creating the instantaneous positive current. The droplet's surface charge density influences how much charge is transferred to the Cu, which in turn affects the device's output. When a water droplet leaves the film surface, it creates a negative electric charge, inducing electron flow from the Cu to ground and producing an instantaneous negative current until equilibrium is re-established.

It was further explained that in case the droplet and the PTFE are neutral and do not carry any charges, to ensure that the water-TENG operates through the coupled effects of triboelectric charge generation and electrostatic induction. Upon a water droplet contacting and sliding on the PTFE, triboelectric charges form at the liquid-solid interface, resulting in a PTFE surface with negative charges and an EDL with positive charges in the adjacent region of the droplet. When the droplet leaves the surface, negative charges build up between the Cu and the ground, causing electrons to flow from the Cu to the ground until the charges balance, creating a peak negative current. Owing to the long-lived triboelectric charges retained on the surface, subsequent droplets are polarized upon contact, re-forming the EDL and creating a disequilibrium positive potential. This reverses the electron flow from the ground to the Cu until a new system is balanced and then generates an instantaneous positive current. Through periodic droplet impact, electrical output occurs continuously.

3.2. Electric Double Layers

The EDL describes how charged surfaces affect charge distribution and the potential difference at the interface between a liquid and a solid, arising from the charged solid interacting with ions in the liquid [12]. The EDL often forms when a liquid comes into contact with a solid surface [22,23]. Nevertheless, conventional EDL models do not explicitly explain how the solid surface becomes charged before EDL formation, where electron transfer is an important process to consider during the electrification that happens when a liquid comes into contact with a solid surface. To provide clarification, Wang et al. introduced a hybrid EDL model as well as explained EDL formation through a "two-step" approach [11,24,25]. In the first step, when solution molecules first encounter a pristine solid surface without pre-existing charges, direct interfacial interactions can induce substantial electron-cloud overlap, leading to initial electron transfer and the generation of charged surface species (Figure 3a (left image)). Under liquid flow or turbulence, molecules adjacent to the surface may detach by breaking interfacial bonds, leaving immobilized ions on the solid surface and releasing counterions into the liquid as mobile ions. In the second step, in the presence of ionic species such as H^+ and OH^-, electrostatic interactions cause oppositely charged ions in the liquid to accumulate near the initially charged surface, forming the EDL (Figure 3a (right image)). Accordingly, EDL formation can be viewed as a subsequent outcome of the initial contact electrification step, in which electron transfer first generates the surface charges that drive interfacial ionic redistribution.

Charge transfer during CE at liquid-solid interfaces is widely explained by the electron cloud potential-well model (Figure 3b (left image)). Within this concept, atoms or molecules are described as potential wells that localize electron clouds in a limited area, while valence electrons remain weakly bound within each well. Prior to contact, electrons remain trapped and cannot transfer across materials. Upon contact between water and a dielectric surface, interfacial screening and electron-cloud overlap break the initial symmetry of the potential well, creating an asymmetric double-well configuration that enables electron tunneling from the liquid to the solid. Simultaneously, as displayed in Figure 3b (right image), thermally driven collisions of water molecules and solvated ions with the surface promote electron transfer and interfacial ionization. The dielectric surface experiences electronic polarization and partial ionization, leading to localized surface charges, the inner Helmholtz

plane (IHP), while redistributed ions create the outer Helmholtz plane (OHP); in concert, these two regions form the Stern layer, where the majority of the interfacial potential drop is localized, with a diffuse layer extending into the bulk liquid to complete the electric double layer (EDL) [26].

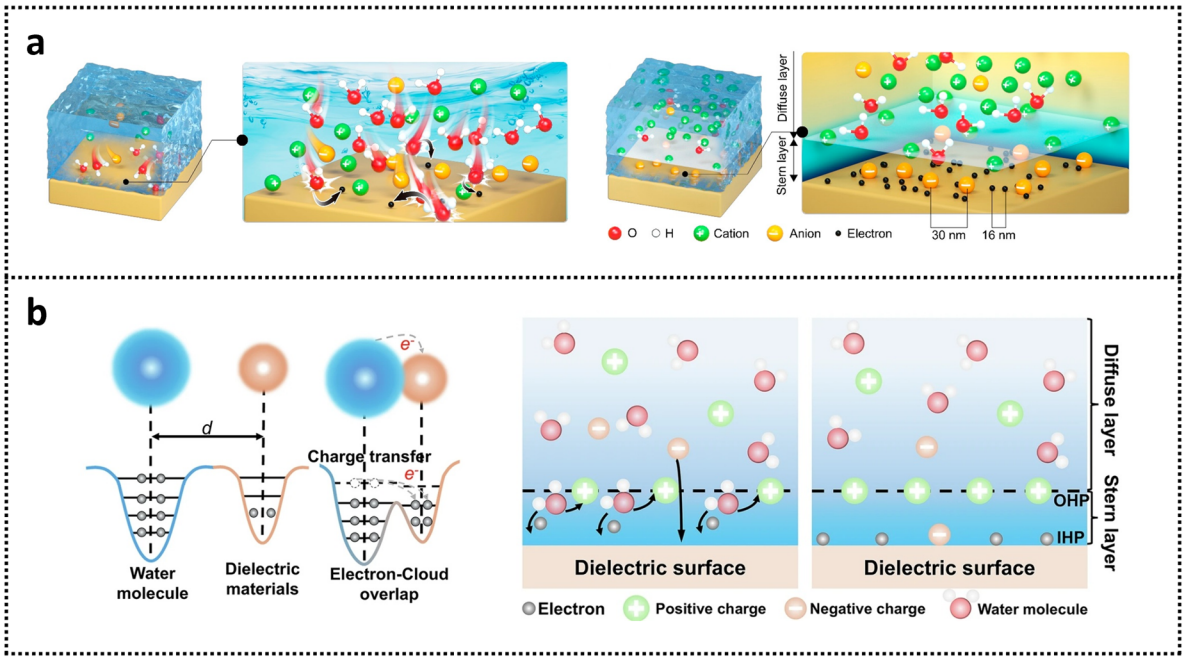

Figure 3. The working mechanisms of D-TENGs. (**a**) Two-step hybrid model for electric double layer formation. Initial electron transfer and ion adsorption at the liquid–solid interface driven by molecular/ionic impact (left). Electrostatic attraction of free ions to the charged surface, leading to electric double layer formation (right). Reproduced with permission from ref. [25]. Copyright 2021 American Chemical Society. (**b**) Illustration of the electron-cloud potential-well model (left image). Two-step model of CE-driven EDL formation with the inner and outer Helmholtz planes (right image). Reproduced with permission from ref. [26]. Copyright 2025 Wei et al. under a Creative Commons license CC BY-NC-ND 4.0, Springer Nature.

Recent studies indicate that liquid-solid contact electrification should be understood as a coupled interfacial charge-conversion process rather than a single charge-transfer mechanism. On residue-free superhydrophobic surfaces, the polarity and magnitude of liquid charging can be regulated by the work-function difference between the liquid and solid, providing strong evidence for electron-transfer-dominated contact electrification under conditions where ion residues are suppressed [27]. In aqueous and dielectric systems, however, this initial charge imbalance is rapidly reorganized by water-dipole orientation, ion adsorption, and EDL formation; recent triboiontronic and triboelectric-probe studies further show that EDL dynamics can actively regulate ion migration and interfacial charge evolution at non-conductive surfaces [26,28]. Therefore, in droplet-TENGs and DEGs, contact electrification should be viewed as the charge-generation step, EDL evolution as the redistribution and screening step, and electrostatic induction as the macroscopic transduction step that converts the evolving interfacial potential into external current. This coupled framework also accommodates emerging evidence that liquid-solid charge transfer can trigger radical formation, H_2O_2 generation, and hidden interfacial electric fields, while high-field regions near the three-phase contact line may induce electrostatic breakdown and limit charge retention [29–31]. Overall, rather than treating CE, EDL formation, and EI as separate mechanisms, liquid-solid droplet electricity harvesting should be described as a coupled interfacial charge-conversion process in which CE generates the initial charge imbalance, EDL evolution redistributes and screens this charge, and electrostatic induction converts the resulting time-varying interfacial potential into external electrical output.

3.3. Hydrovoltaic Effect

The hydrovoltaic effect describes electricity generation arising from the interaction between water and solid materials, particularly nanostructured surfaces, where interfacial electric double layers play a central role [32,33]. Within this framework, the drawing potential represents a specific electrokinetic mechanism in which the motion of an ionic droplet across a conductive surface (e.g., graphene) dynamically charges and discharges a pseudocapacitor at the droplet-solid interface, producing a voltage proportional to the droplet velocity (*v)* and

droplet number (n), following $V, I \propto n\ C_0 v$, where C_0 is the pseudocapacitance per unit area [33]. This mechanism can be extended to harvest energy from raindrops, where the splash of a falling droplet onto a tilted graphene surface produces a voltage nearly an order of magnitude larger than that generated by drawing a droplet of comparable size, owing to the rapid spreading dynamics during impact.

3.4. Tribovoltaic Effect

The tribovoltaic effect is an interfacial charge-generation mechanism observed at semiconductor-containing junctions, analogous to the photovoltaic effect, where electron-hole pairs are excited by photons. In the tribovoltaic effect, energy from contact electrification and bond formation (bindington) excites electron-hole pairs, instead of using light to stimulate them. Additionally, at liquid-semiconductor interfaces, the tribovoltaic effect can take place, in which the liquid phase acts as a semiconductor-like medium, forming a heterojunction with the solid surface [24]. Lin et al. set up the experiment in which the DI water droplet was dragged over a silicon surface using a conductive needle [34]. They observed a positive current when the droplet slid over p-type silicon, indicating electron movement from silicon to water. In contrast, a negative tribo-current was generated on n-type silicon, showing electron movement in the opposite direction. Additionally, Zheng et al. [35] further found that light irradiation enhances the tribo-current at the interface between liquid and solid by increasing charge-carrier pairs. Carriers are separated by the built-in field, with electrons and holes moving in opposite directions in p-type and n-type semiconductors, whereby confirming the occurrence of the tribovoltaic effect at liquid-solid interfaces [35]. Mechanistically, the process occurs in sequence: first, when water contacts a semiconductor, a liquid-semiconductor junction forms due to the Fermi-level difference, establishing a built-in electric field at the interface. During sliding, collisions between water molecules and surface atoms promote electron-cloud overlap, enabling electron transfer and/or bond formation at freshly contacted surface sites. The released interfacial energy, bindington, excites electron-hole pairs near the surface of the semiconductor. The built-in field then drives charge separation, causing electrons and holes to migrate in opposite directions according to the conductivity type of the semiconductor, whether p-type or n-type, which determines the polarity of the measured tribo-current and tribo-voltage. This behavior supports electron transfer as the key initial step in liquid-solid CE, consistent with the hybrid two-step EDL model.

Recently, Li et al. [36] have developed a Schottky metal-semiconductor-metal (MSM)-based tribovoltaic nanogenerator (MSM-based TVNG), transforming droplet kinetic energy to direct current electricity. In the Schottky MSM-based TVNG, electricity generation arises from droplet-triggered modulation of a static Schottky barrier rather than from a conventional dynamic sliding metal-semiconductor junction. Given that the sputtered bottom Pt/p-Si interface behaves nearly as an ohmic contact with minimal resistance, the MSM device can be simplified as a diode in series with a resistor, representing the top and bottom junctions. As a water droplet impacts the p-Si surface, bridges to the top Pt electrode, and finally departs, electrical output emerges through two sequential dynamic excitations. Upon initial impact, gravitational potential energy turns to kinetic energy, while interfacial contact electrification drives electron transfer from p-Si to water, leaving the droplet negatively charged and the p-Si surface positively charged. The resulting cationic region electrostatically induces negative charges in the top Pt electrode, thereby forward-biasing the top Schottky barrier and driving current from p-Si to Pt. A second excitation arises when the droplet directly contacts the top Pt electrode; electrons are transferred from water to Pt, further charging the Pt negatively and directly lowering the Schottky barrier to sustain current flow from p-Si to Pt. Once the droplet leaves the MSM structure, the induced bias collapses, and the output vanishes.

At thermal equilibrium, the top junction has a much larger Schottky barrier height and width than the bottom ohmic-like contact, producing a built-in electric field E_1. During the first excitation, the top barrier on the p-Si side is lowered, and the built-in field weakens to E_2, allowing holes in p-Si to move toward Pt. Meanwhile, the barrier also becomes thinner. After the second excitation, the built-in field further decreases to E_3, together with an additional reduction in both barrier height and thickness. Once the droplet leaves the device, the top Schottky junction recovers its equilibrium state. In contrast, metal-oxide-semiconductor-based devices behave more like transistors, where electricity generation mainly arises from electrostatic induction and the output is typically alternating current.

To clarify the overlapping roles of different interfacial processes, Table 1 summarizes the conditions under which each mechanism is expected to dominate in droplet-TENGs and related droplet-electricity devices.

Table 1. Comparative summary for droplet-TENGs and related droplet-electricity devices.

Conditions	Likely Dominant Mechanism	Ref.
Fresh or residue-free superhydrophobic dielectric surface; droplet rebounds cleanly with minimal ionic residue.	Contact electrification (electron-transfer-dominated)	[27]
Initial liquid-solid contact on a hydrophobic dielectric in a classical droplet-TENG.	Contact electrification initiates interfacial charging	[27,30]
Aqueous electrolyte droplet remains on the surface long enough for ion redistribution and water-dipole orientation.	Electrical double layer (EDL) formation/interfacial screening	[26,28]
Electrolyte chemistry actively modulates transient interfacial charge transfer and ionic rearrangement.	Coupled CE + EDL, with EDL-dominated regulation	[26,29]
Droplet motion changes the contact area, or a droplet temporarily bridges electrodes in a precharged device.	Electrostatic induction (main output transduction step)	[30]
Very high local field at the liquid–solid–gas triple-phase contact line; small gap or sharp geometry.	Electrostatic induction with breakdown/discharge assistance	[31]
Continuous sliding or flowing liquid on carbon, 2D, or porous materials, outside a classical dielectric droplet-TENG architecture.	Hydrovoltaic effect	[32,33]
A droplet interacts with a semiconductor, Schottky, or junction-type interface, where a built-in field is essential.	Tribovoltaic effect	[24,34–36]
Most practical droplet-TENGs with polymer dielectric and electrodes.	CE generates charge, EDL redistributes/screens it, and EI converts it into measurable output	[29,30]

4. Energy-Harvesting Devices' Performance

4.1. Metrics for Device Performance Comparison

Comparing the performance of D-TENGs and DEGs is crucial for identifying true advancements in droplet-energy conversion, as careful evaluation helps differentiate real progress from variations due to test conditions or device design, aiding both understanding and development. Droplet electricity-harvesting devices are tested under different conditions, making it hard to compare their performance. Focusing on their actual capabilities and avoiding any confusion that may arise from the testing methods employed is essential. The metrics in Figure 4 indicate the actual amount of useful electrical energy extracted from a single droplet. The primary criterion is energy per droplet (E_{out}), which indicates the actual electrical energy obtained from a single droplet at a specific external load resistance (R_L). Thus, it provides a more significant evaluation of usable output than merely peak voltage or current, and can be calculated by the following equation over the duration of a single droplet-induced pulse (t_1 to t_2) [37]:

$$E_{out} = \int_{t_1}^{t_2} \frac{V(t)^2}{R_L} \mathrm{d}t = \int_{t_1}^{t_2} I(t)^2 R_L \, \mathrm{d}t = \int_{t_1}^{t_2} V(t)\, I(t) \mathrm{d}t \quad (1)$$

where $V(t)$ and $I(t)$ are the voltage and current across the R_L. The second criterion is energy conversion efficiency, η, which evaluates how efficiently the mechanical energy of an impinging droplet is converted into electrical energy. It is generally expressed as an Equation (2):

$$\eta = \frac{E_{out}}{E_{in}} = \frac{\int_{t_1}^{t_2} \frac{V(t)^2}{R_L} \mathrm{d}t}{mgh} \quad (2)$$

where E_{in} represents the droplet input energy, calculated from gravitational potential energy (mgh), where m, g, and h are the droplet mass, gravitational acceleration, and release height, respectively. If the impact velocity (v) is directly measured, E_{in} may alternatively be estimated from impact kinetic energy ($\frac{1}{2}mv^2$) [38,39]. Although energy conversion efficiency indicates how efficiently a device transforms available mechanical energy into electrical energy, viscous and electrical losses can significantly restrict this conversion, even in devices operating at high voltage [38]. The third metric, power density, is an important application-oriented parameter for droplet electricity harvesting because it describes how rapidly the harvested electrical energy can be delivered to an external load after normalization to an active or device area. Unlike open-circuit voltage, which only reflects the maximum

electrostatic potential under negligible current flow, power density must be evaluated under a connected load resistance, preferably at the matched-load condition. The instantaneous peak power (P_{peak}) and the instantaneous peak power density ($P_{peak,d}$) under an external load resistance can be expressed as in Equations (3) and (4), respectively:

$$P_{\mathrm{peak}} = \frac{V_{\mathrm{max}}^2}{R_{\mathrm{L}}} = I^2 R_{\mathrm{L}} \tag{3}$$

$$P_{\mathrm{peak,d}} = \frac{P_{\mathrm{peak}}}{A_{\mathrm{eff}}} = \frac{V_{max}^2}{R_{\mathrm{L}} A_{\mathrm{eff}}} = \frac{I^2 R_{\mathrm{L}}}{A_{\mathrm{eff}}} \tag{4}$$

where A denotes the effective liquid-solid contact area, maximum droplet spreading area, or electrode-overlap area used for normalization. For fair comparison, the definition of A must be explicitly stated. In many reports, the maximum power is obtained by testing different load resistances and identifying the matched load that gives the highest instantaneous power. However, because droplet generators produce short and pulsed outputs, peak power density alone may overestimate practical performance. Therefore, peak power density should ideally be reported together with average power density ($P_{avg,d}$) [40], calculated by integrating the load power over a defined time window and normalizing it by the effective working area (A_{eff}), as shown in Equation (5).

$$P_{\mathrm{avg,d}} = \frac{E_{out}}{A_{\mathrm{eff}} T} = \frac{1}{A_{\mathrm{eff}} T} \int_0^T \frac{V(t)^2}{R_{\mathrm{L}}} \mathrm{d}t \tag{5}$$

The distinction between peak and average power density is essential because droplet-TENGs and DEGs can generate high-voltage pulses on a millisecond timescale, whereas practical energy supply depends on the amount of energy that can be repeatedly collected, rectified, and stored. The last metric is charge density, which quantifies the amount of charge generated, stored, or transferred at the droplet-solid interface per normalized area. In droplet-TENGs and DEGs, the total transferred charge per droplet is obtained by integrating the current pulse [36]:

$$Q_{tr} = \int_{t_1}^{t_2} I(t)\, \mathrm{d}t \tag{6}$$

and the areal charge density is defined as:

$$\sigma_A = \frac{Q_{\mathrm{tr}}}{A_{\mathrm{eff}}} = \frac{\int_{t_1}^{t_2} I(t)\, \mathrm{d}t}{A_{\mathrm{eff}}} \tag{7}$$

Charge density is increasingly reported either as an areal metric, Q_{tr}/A_{eff}, for planar droplet-impact devices, or as a volumetric metric, Q_{tr}/V_{drop}, for confined, floating, or three-dimensional droplet generators, where the effective interfacial area is difficult to define.

Table 2 enables the comparison of devices' performance with different structures by summarizing charge output, charge density, energy per droplet, energy conversion efficiency, power density, external load resistance, and current type. Various droplet categories can produce significantly different electrical outputs, even when utilizing the same device structure, highlighting the considerable impact of droplet chemistry on charge generation and energy conversion. Moreover, a higher charge density does not necessarily translate into a higher power density, indicating that droplet-based generators should be evaluated using multiple performance metrics rather than a single output parameter. The transferred charge (Q_{tr}) and charge density (σ) describe the charge-generation and charge-collection capability, whereas energy per droplet (E_{out}) and conversion efficiency (η) more directly indicate the ability to convert droplet mechanical energy into usable electrical energy. Power density (P) further reflects the instantaneous energy-delivery capability under an external load. Nevertheless, direct comparison remains limited because the devices are tested with different droplet chemistries, droplet volumes, load resistances, output modes, and area-normalization methods. Therefore, Table 2 is useful for identifying performance trends, but a fair device ranking requires standardized reporting of matched-load power, energy per droplet, charge density, conversion efficiency, droplet conditions, and active-area definitions.

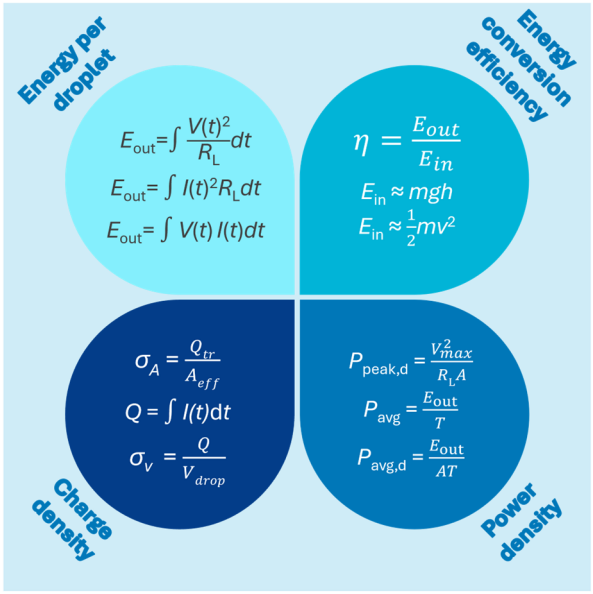

Figure 4. Metrics for device performance comparison.

Table 2. Comparison of devices' performance with different structures.

Device Structures	Types of Droplet	Droplet Volume (μL)	Q_{tr} (nC)	Charge Density (C/m^3)	Energy (μJ)	Energy Conversion Efficiency	Power Density (W m^{-2})	External Load Resistance (kΩ)	Types of Electric Current (AC or DC)	Ref.
F-LIG/FEP-PI/LIG	Water	105	71.8	0.684	5.9	2.29%	47.5	360	AC	[41]
Al/PFDTMS+PTFE/ITO	Tap water	90	500	5.56	-	-	-	300,000	AC	[42]
	DI water	90	80	0.89	21.03	14.02%	-	100,000		
Al/PTFE/ITO/glass	Tap water	100	49.8	0.498	3.2	2.2%	50.1	332	AC	[37]
PFDTMS-grafted, sandpaper-roughened PDMS/ITO/glass/Al	DI water	100	90–100	0.90–1.00	34.6 (30 MΩ)	17.1% (30 MΩ)	2.23	20,000	AC	[43]
Steel/FEP/MWCNT-PMDS/ITO/Glass	Tap water	72	40	0.556	5.23	4.96%	487.93	200	AC	[44]
Cu/Pt needle/PTFE/Cu	DI water	80	4.5	0.056	2.8	2.4	-	-	DC	[39]
Cu/Pt needle/Cu/FEP/Cu	DI water	100	30	0.3	2.2 (μJ/cm^2)	-	-	-	DC	[45]
Pt/Polarized PZT/Pt	1M NaCl	55	650	11.82	-	3.28	5.3	1	DC	[46]
Al/FEP/Au	DI water	100	700	7.0 (13.926 mC/m^2)	-	-	-	-	DC	[47]
Pt/SiO_2/p-Si/Pt	NaOH (pH = 14)	73	25,500	349	79.4 (J/m^3)	11%	-	51	DC	[36]

Note: F-LIG = F-doped Laser-induced graphene.

4.2. Output Performance Improvement Strategies

Enhancing D-TENGs and DEGs performance requires an understanding of the mechanisms governing the fabricated devices, the properties of materials used, and the devices' structure. Insight into the mechanisms is key to optimization; choosing the right materials is essential, as surface chemistry, conductivity, and wettability can affect the electrical output. Furthermore, the structure's design matters because it influences how droplets spread and separate, which in turn affects contact time, charge separation, and energy efficiency. Mechanistic insight, materials design, and structural engineering are strategies repeatedly used to improve the efficiency of droplet electricity-harvesting devices.

4.2.1. Mechanistic Insight

In conventional droplet-based TENGs, electricity generation is limited to interfacial contact electrification, resulting in minimal charge extraction and suppressed current. Instead, Xu et al. [37] fabricated a DEG that bridges the charge-loaded PTFE/ITO region and Al electrode, switching the system from an open to a closed circuit. During the early spreading stage, minimal current is produced. Once the droplet contacts the Al electrode, a rapid charge transfer from ITO to Al occurs, resulting in a sharp current peak. As the droplet maximally spreads, the charge transfer peaks. When the droplet retracts, the current reverses, indicating a return flow from Al to ITO, resetting the cycle upon detachment. This suggests that the DEG transforms an effect at the surface into an effect throughout the entire material, driven by transient capacitor formation at the water/PTFE interface and water/Al interface. However, the mechanism underlying this DEG remains ambiguous. Wang et al. [48] systematically investigated a repeatedly operating DEG by correlating high-speed camera observations with electrical output to establish a dynamic surface-charge-density model that clarifies its working mechanism. The working mechanism is mainly governed by the dynamic modulation of surface charge density. The PTFE film stores stable negative charges, which electrostatically induce positive charges on the two electrodes; at equilibrium, the top-electrode charge density satisfies $2\sigma_{top} = \sigma_{PTFE}$. When a conductive droplet contacts the top electrode and spreads, the liquid surrounding the electrode can be treated as an equivalent extension of the top electrode area. This added area, ΔS, lowers the positive surface charge density on the top electrode and disrupts electrostatic balance, thereby driving electrons from the top to the bottom electrode until equilibrium is re-established. The model further shows that the generated current and voltage are proportional to the droplet area change rate, dS/dt, indicating that the output is controlled primarily by the speed of interfacial evolution during spreading rather than by droplet area alone. When the droplet subsequently shrinks, ΔS decreases, the top-electrode charge density rises again, and electrons flow in the reverse direction, producing the backflow pulse. Thus, electricity generation originates from the time-dependent expansion and contraction of the droplet-defined effective electrode area, which periodically perturbs and restores the electrostatic equilibrium of the device.

Inspiration from nature, the electric ray, Dong et al. fabricated a device that creates a new way to harvest energy from water droplets [49]. The device transforms droplet energy harvesting into charge pumping rather than simple induction. Conventional droplet TENGs are fundamentally based on the classic CE and EI framework of TENGs, whose operation relies on the interfacial electrostatic field and Maxwell displacement current. The work by Li et al. [45] still uses CE and electrostatic transduction but adds a capacitive-coupling enhancement mechanism, enabling displacement-current-assisted storage and conduction-current-assisted transfer to cooperate, thereby increasing both the maximum stored charge during contact electrification and the conversion efficiency during electrostatic transduction. The key innovation is a back-gate electrode inserted beneath the FEP layer, creating a MOSFET-like modulation geometry that converts a surface-limited total current droplet-based nanogenerator into a bulk-effect-enabled system.

Leveraging the barrier-induced built-in electric field of Schottky contacts, Li et al. [50] fabricated a Schottky MSM device capable of generating a direct current of up to 400 μA from a single water droplet. By using a triboelectrically gated Schottky-MSM mechanism, a water droplet transfers electrons from p-Si to water and, with temporarily bridging p-Si and the Pt electrode, applies an effective bias that lowers and narrows the top Schottky barrier, achieving directional hole transport and generating pulsed DC output without an external rectifier [50]. Li and colleagues [36] further developed a Schottky-MSM device for harvesting electricity from droplets, but with a different mechanism. The two distinctive concepts of operating modes in a Schottky-MSM device are static and dynamic junctions. In the static case, the junction already exists as a fixed device architecture; in the dynamic case, the junction is effectively activated during interfacial motion. The static Schottky-MSM device is asymmetric, where the top Pt/p-Si contact functions as a Schottky junction, while the bottom contact is ohmic-like, providing rectifying behavior and designating one interface as the primary transport barrier. In the energy-band diagram of the static Schottky-MSM, the top Schottky contact creates a depletion region and a built-in electric field directed

from Pt to p-Si, resulting in band bending and establishing the interfacial barrier that regulates carrier motion. During contact between Pt and p-Si, electrons transfer from p-Si to Pt because of their electronegativity difference, leaving p-Si positively charged and Pt negatively charged after separation. In the dynamic Schottky metal-semiconductor junction, contact-electrification-induced interfacial fields can overcome the built-in field, thereby modulating the Schottky barrier and driving tribovoltaic carrier transport rather than conventional electrostatic-induction-based generation. Apart from triboelectrification, electrostatic induction, triboelectric effect, and hydrovoltaic effect, Wang et al. [51] induced a droplet electrochemical cell (DECC) based on a Zn-Cu primary-battery-like configuration, in which impinging water or electrolyte droplets bridge two metal electrodes to directly harvest droplet energy with enhanced current (400 μA) and charge output (3.2 μC).

4.2.2. Materials Designs

The surface molecular structure of the triboelectric layer plays a critical role in determining droplet TENG efficiency. Meng et al. [42] modified the PTFE triboelectric layer with fluorosilane (1*H*,1*H*,2*H*,2*H*-perfluorodecyltrimethoxysilane (PFDTMS)), enhancing the triboelectrification sites and improving electron transfer at the interface between liquid and solid, leading to increased device performance. Similarly, Zhang et al. [43] grafted PFDTMS onto sandpaper-treated polydimethylsiloxane (PDMS) film, achieving a 10–20 fold improvement in voltage, current, and charge compared to the untreated PDMS-based device. Additionally, Hu et al. [52] employed silicone resin instead of fluorinated polymers as the friction layer and studied how engineered surface wettability influences droplet-based electricity generation. The generated electrical output increased nearly 700-fold at an optimal contact angle of 98° but declined at higher contact angles. Furthermore, Min et al. [53] examined the interplay between surface hydrophobicity and stickiness by incorporating carnauba wax (C-wax) into the PDMS film. They found that reduced surface stickiness (lower contact angle hysteresis) enhanced droplet spreading and contraction dynamics. This improvement was attributed to the formation of C-wax-induced microstructures that minimized water-PDMS adhesion, thereby increasing the electrical output.

Composite materials are widely used to tailor dielectric properties and enhance the performance of droplet-based TENG devices. Mai et al. [54] used a nanocomposite of amorphous fluoropolymer films doped with polytetrafluoroethylene particles as the dielectric layer to improve the device performance. In addition, Chen et al. [55] introduced interfacial polarization through a dielectric-contrast composite design and plasma surface treatment that enhanced polarization and charge trapping, thereby achieving 448 W m^{-2} of instantaneous peak power density without pre-charging assistance. A bilayer dielectric made of perfluoropentylglyoxal ($C_7F_{12}O_2$) and PTFE, together with a plasma-modified interface, is designed to create permittivity-mismatch-induced interfacial polarization, which adds an extra electric field and enhances triboelectric output. The modified-interface device produces much higher peak power than the untreated one. Apart from composite materials, hydrogels have been leveraged to fabricate hydrogel-based droplet electricity generators due to their intrinsic optical transmittance (≈99%) and stretchability (≈70%), which enable seamless integration onto various surfaces [56].

Conventional polymer-surface-based droplet harvesters struggle with low surface charge density, unstable charges, and limited compatibility with ionic droplets; hence, inorganic materials are considered to alleviate these limitations. Certain ferroelectric oxides, such as lead zirconate titanate (PZT), are attractive owing to their polarized surfaces, which generate large fixed charges that generally exceed triboelectric charge densities, thereby improving output stability and facilitating the electrostatic separation of positively and negatively charged ions for generating direct current (Figure 5a) [46]. Similarly, GaN, an inorganic semiconductor, has high electron mobility and strong resistance to chemicals, heat, and physical stress, helping transfer charge efficiently, keep device resistance low, and ensure reliable performance even during rapid impacts from droplets [57]. Thereafter, inorganic compounds are valuable for increasing output, enhancing durability, and broadening the functions of droplet-based electricity harvesters.

As environmental concerns drive the use of sustainable materials, recycled materials are gaining attention for their sustainability benefits and reduced fabrication costs. Wang et al. [58] fabricated a device using a recycled DVD, which was motivated not only by the desire to replace expensive or synthetically demanding components with an inexpensive and readily available alternative, but also by the presence of a nanograting structure that can facilitate charge trapping and thereby enhance device output. Such an approach highlights that the integration of recycled materials can serve as both a sustainable fabrication strategy and a route to high-performance droplet energy conversion.

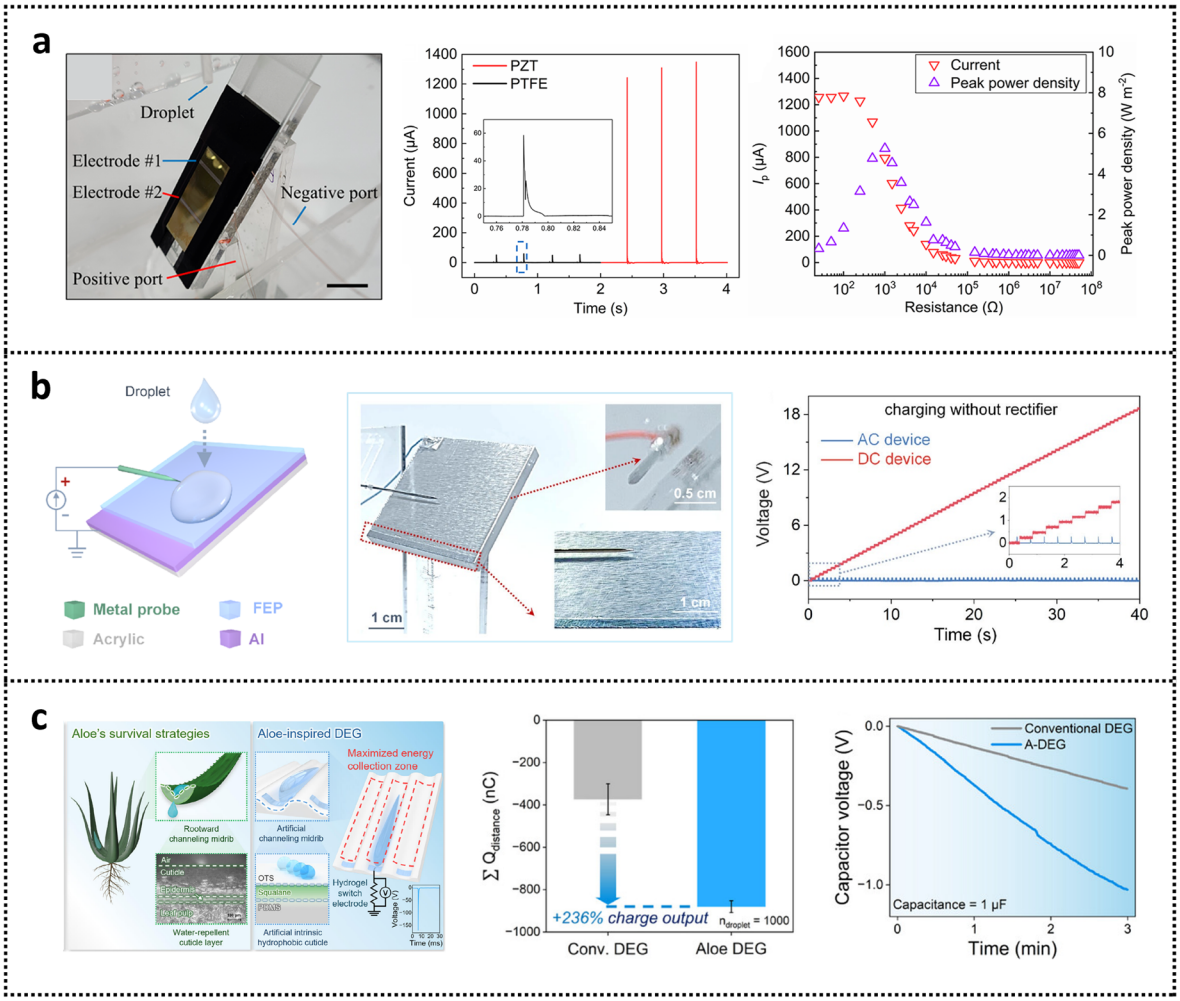

Figure 5. Material and structural design used to improve devices' efficiency. (**a**) The optical image of the device structure made of PZT film and its electrical outputs. Reproduced with permission from ref. [46]. Copyright 2023 American Chemical Society. (**b**) Optical photograph of the device with a suspended probe and an exposed bottom electrode**.** Reproduced with permission from ref. [59]. Copyright 2025 Elsevier Ltd. (**c**) Conceptual diagram of the device inspired by the Aloe's survival approach in the arid desert and the output performance. Reproduced with permission from ref. [60]. Copyright 2026 Lee et al. under the terms of the Creative Commons Attribution License, Wiley-VCH GmbH.

4.2.3. Structural Engineering

To overcome the low output of conventional single-electrode-mode droplet TENGs, which limits their real-world applications, many researchers have modified the structure by adding an electrode, reducing electrode size, and changing electrode position. For instance, Zhao et al. [61] fabricated a D-TENG with a bi-electrode by controlling droplet impact positions to maximize current, and proposed a mechanism involving charge transfer caused by an uneven distribution of capacitance that accounts for the enhanced output. Also, Wang et al. [62] improved the conventional device efficiency by co-optimizing the inductive electrode size and the dynamics of droplet impact, spreading, and sliding. Structurally, a PTFE dielectric layer covers a copper electrode that has a smaller size than the PTFE film. Furthermore, Meng et al. [63] developed a D-TENG in a single-electrode mode to eliminate the complicated encapsulation process in fabricating a device and facilitate performance enhancement, which differs from conventional devices by depositing an electrode on the dielectric layer rather than at the bottom. The device can generate the current output up to 3mA owing to its top-electrode architecture, which enables direct droplet-electrode coupling, suppresses interfacial shielding and charge dissipation, and thereby converts triboelectrically generated surface charge into efficient bulk charge transfer. Additionally, to better understand charge-transfer processes, Prendergast et al. [64] introduced a point-electrode TENG to elucidate how electrode placement, droplet dynamics, and dielectric-surface design influence output and can be optimized for higher-efficiency architectures.

Since the alternating-current output from droplet-based generators is low and insufficient for practical use, this is due to the fact that only a small quantity of interfacial charge is produced, and an even smaller amount is effectively harvested during the short and inefficient process of droplet impact [11]. Dong et al. [39] demonstrated a direct-current device that integrates rectification, energy conversion, and storage into a single device to mitigate inevitable energy loss. The device produces two pulse peaks with one droplet, where a pulse peak I is generated when the expanding droplet first touches the charge-collector needle and closes the circuit, whereas Peak II arises when the droplet subsequently moves downward to contact the bottom electrode, reconnecting the circuit and producing a second pulse in the same current direction. Another direct-current device was developed by Bao et al. [59], featuring a suspended electrode in air and an exposed lower part of the bottom electrode, resulting in a transferred charge of 32.5 nC per droplet (Figure 5b). In this suspended-needle device, the droplet detaches from the upper probe before the lower electrode can recharge, so the reverse-current peak is eliminated, and the residual positive charges in the droplet move unidirectionally to the exposed lower electrode, producing DC output.

Due to interface-effect limitations in traditional droplet-based TENGs, Xu et al. [37] introduce a simple device consisting of PTFE deposited on ITO glass and an aluminum electrode mounted on top of the PTFE film, which converts the typical interfacial effect into a bulk effect, achieving an elevated output when droplets impinge on the device. That established a new mechanistic framework and a significantly higher power-density standard for subsequent droplet-based generator research. Previous DEG designs are usually based on a single dielectric layer, which restricts their integration into everyday surfaces. Hence, Wang et al. [65] proposed a multilayer dielectric device for practical water-energy harvesting by integrating a triboelectric surface with common materials such as glass and umbrella fabrics. This design enhances equivalent capacitance and interfacial charge density, significantly increasing electrical output. Additionally, Ying et al. [66] proposed a three-layer DEG to improve its performance by adding an electron-trapping layer (WO_3) between an aliphatic polyimide and a fluoropolymer. A single droplet of water (50 μL) can generate a peak power of 2.7 mW when impacting on this multi-layer device. Notably, Wang et al. [67] reported the first incorporation of high-entropy ceramics into the DEG intermediate layer design, yielding a substantial output voltage of 525 V. The enormous dielectric constant of high-entropy ceramics can help minimize the decay of triboelectric charges in DEG.

Beyond multilayer structure devices, Lee et al. [60] fabricated a device inspired by Aloe vera (Figure 5c (left image)) that can withstand harsh conditions to overcome a key limitation of conventional DEG, which is that the energy harvesting is confined to a narrow region near the switch electrode, making performance highly sensitive to the droplet's impact location. The device features a curved midrib that guides droplets in one direction and an artificial cuticle made of octadecyltrichlorosilane-squalane that helps the droplets slide smoothly without getting stuck. When a droplet hits the surface, it generates charges at the water-cuticle interface. When the droplet reaches the hydrogel switch electrode, it completes the circuit, allowing the stored energy to discharge. This bioinspired design greatly increases the area where energy can be collected and provides about 236% more charge output compared to traditional generators (Figure 5c (middle image)). The comparison of the charging behavior of the Aloe-inspired DEG and the conventional DEG under the same conditions is shown in Figure 5c (right image), where the Aloe-inspired DEG performs better than the conventional one.

When the droplets touch the ambient water, the device's performance decreases. To solve this problem, Shao et al. [68] introduced a device using a field effect to store a high volume of charge in a triboelectric layer, causing the improvement of instantaneous power density and energy conversion upon the impingement of droplets. Also, direct droplet-electret contact may cause performance deterioration in traditional devices. Deng et al. [69] introduced a contactless D-TENG that transduces droplet stimuli into electrical energy or signal outputs continuously and stably without requiring direct droplet contact.

As the electricity generated by single-mechanism nanogenerators alone is insufficient to power practical applications, researchers have integrated multiple mechanisms into a single device to increase overall electrical output and address this obstacle [70]. For instance, Kam et al. [71] developed a 4D-printed elastic hybrid device that combines a DEG with a solid-solid TENG. In this design, a single droplet impact simultaneously drives the DEG and deforms the elastic structure, allowing part of the otherwise dissipated mechanical energy to be converted into additional triboelectric output. Compared with a single DEG device, the total output and energy-supply performance of this hybrid device improved by about 30% and 25%, respectively. Similarly, Liu et al. [72] developed a dual-mode triboelectric nanogenerator that converts both interfacial electrostatic energy and elastic potential energy from droplet impacts. The droplet's impact stimulates multiple vibrations in a flexible cantilever, enhancing charge output through frequency multiplication. A top electrode effectively bridges interfacial charges, optimizing energy extraction, and triggered by a single droplet, the device delivered a total transferred charge of up to 158 nC. In addition, to harvest raindrop energy more effectively, Zhang et al. [73] proposed a flexible droplet-based hybrid device that combines a DEG with an EMG. The two units were integrated using a conductive elastic

MWCNTs/PDMS film, which serves as both the DEG bottom electrode and the elastic component that drives EMG vibration upon droplet impact, allowing a single droplet to trigger dual electricity-generation pathways simultaneously, resulting in delivering a peak power of nearly 600 μW. Another dual-mode device by Xie et al. [74] is integrated with a silicon tandem solar cell so that raindrop impact is converted into electricity through both surface single-electrode and contact-separation triboelectric processes, while the silicon cell simultaneously harvests light, thereby compensating for photovoltaic output loss under low-light rainy conditions.

Although transiter-like droplet electricity generators improve the electricity generation of a single-position droplet, designing devices for harvesting energy from multi-position droplets on a large scale is limited. Wang et al. [75] draw inspiration from a honeycomb to fabricate an array of droplet-based generator cells arranged in a honeycomb pattern, where each cell is a tubular and transiter-like structure. The device can generate an average peak V_{OC} nearly twice that of the conventional planar array. Besides, Yang et al. [76] fabricated a multi-position, multi-stacked droplet-based TENG to harvest raindrop energy at practical scales. At the same height, the multi-stacked structure enhanced the output by 38.2% compare to a single-stack device.

Directly linking energy collection and conversion modules often leads to issues such as material wear, spatial scalability limitations in large-scale applications, and reduced energy conversion efficiency. To overcome these challenges, Zheng et al. [77] introduced a remote-controlled energy harvesting strategy using a confined capillary channel. The device spatially decouples mechanical energy collection from electrical conversion. When deforming an elastic cavity, an external force generates pneumatic motion that drives encapsulated water droplets back and forth within slippery FEP capillaries equipped with one source electrode and two drain electrodes. In terms of mechanism, the moving droplet acts as a gate-like conductor that intermittently closes the circuit with each drain, allowing for the sequential capture and release of electrostatically induced charges while preventing charge buildup on repeated droplets, thus enabling effective and scalable electricity generation in confined channels. With the single-unit device, high instantaneous voltage and current can be generated.

5. Applications of Droplet-Based Devices in Electricity Harvesting

D-TENGs and DEGs are increasingly being developed as practical technologies for rain-energy harvesting, scalable array-based collection, direct power delivery to small electronics, self-powered system integration, and chemical or biological sensing, shifting the devices' design from isolated single-droplet demonstrations toward robust architectures that can operate under realistic environmental conditions and deliver more usable electrical functions. A summary of the applications of droplet energy-harvesting devices is shown in Figure 6.

Harvesting energy directly from raindrops and other ambient water-driven mechanical inputs is a major application of D-TENGs and DEGs. The impact of raindrops on engineered liquid-solid interfaces can be converted into high instantaneous electrical output, thereby demonstrating the feasibility of rain as a viable microscale energy source [37]. Following studies extended this concept through direct-current droplet generators, which reduce the need for external rectification and improve the practical usability of the harvested output [39], as well as through needle-electrode [78] and suspended-probe configurations [59] that can convert the energy from falling or sliding droplets into electrical signals more effectively. Furthermore, droplet-energy harvesting from diverse water sources and under harsher chemical environments is also developed, suggesting that droplet-based generators could be adaptable to outdoor and chemically complex environments [68].

Scalable energy harvesting through multiple droplets, array systems, and hybridized device architectures is another important application. Because the output from an individual droplet is inherently discrete and localized, many recent studies have focused on capturing energy from many droplets concurrently through multi-position, multilayered, or array-based designs [62,72,75,76]. However, scaling up droplet energy harvesting remains challenging [79]. Firstly, each DEG cell requires a full-wave rectifier to convert AC output to DC and prevent destructive interference with other DEGs, which increases the cost and complexity of the devices. Secondly, the degradation of the devices' performance due to the large panel-level parasitic capacitance, which is the undesirable capacitance that emerges in an integrated DEG array, particularly when multiple DEG cells are constructed on the same expansive panel and utilize common electrodes or circuit connections. Thirdly, due to the high instantaneous pulsed voltage generated by D-TENGs and DEGs with short pulsed periods (10-ms level), storing the electricity generated by these devices in batteries and capacitors is highly inefficient, with efficiencies of less than 2%. To overcome these challenges, Li et al. [79] presented a generic design strategy that enables high-efficiency energy harvesting in large-scale DEG arrays (Figure 7 (first-row images)). Despite many efforts to reduce parasitic capacitance by shrinking the top-electrode footprint or the overlap area between the two electrodes, the effect of the bottom electrodes has been largely ignored. They found that excessively large bottom electrodes increase parasitic capacitance and thus reduce output power, whereas the output is maximized when the bottom electrode

area is comparable to the maximum spread area of the impinging droplet. Based on this, revising the configuration of the bottom electrode from a global to a localized approach resulted in a nearly fourfold increase in the average power density of individual DEGs. This method enabled the integration of five DEGs into a single panel with one rectifier, generating 85.9 μW, while assembling six of these panels into a 30-cell array yielded 371.8 μW, more than double the output of previous designs. To more effectively store the array's variable output, ultrafast metal-free micro-supercapacitor (MSC) arrays were created, with the fabrication method together with its electrode arrays shown in Figure 7 (second- and third-row images), capturing 21.8% of the peak output power. The integration of large-scale DEG arrays with large-scale MSC arrays is considered a promising approach for practical clean energy harvesting from natural water. Collectively, these developments bring the field closer to practical rain-harvesting surfaces that can collect multiple droplets simultaneously rather than capture them individually.

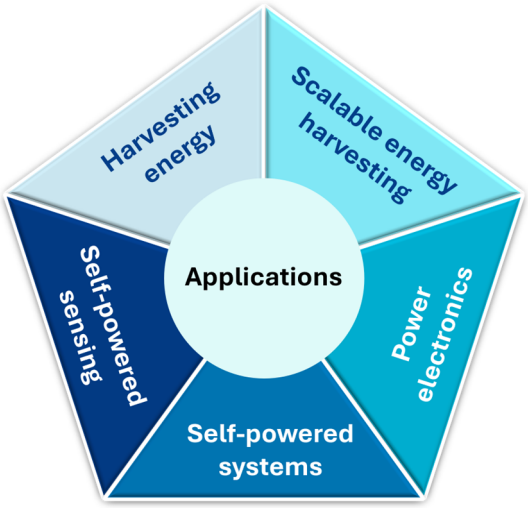

Figure 6. The applications of droplet electricity-harvesting devices.

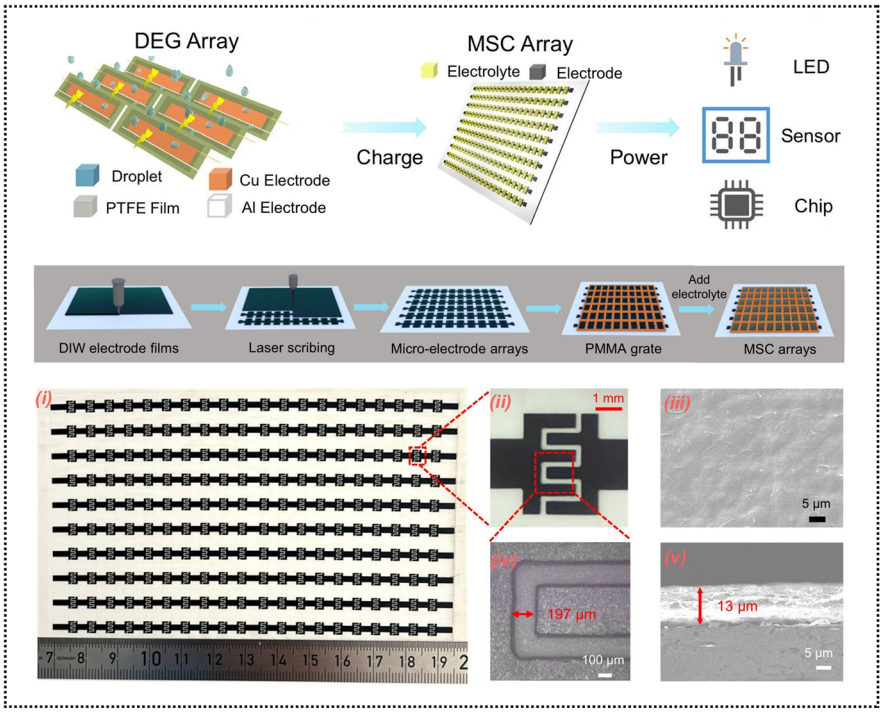

Figure 7. The conceptual images of a self-charging power system. Schematic of the self-charging power systems (SCPS) featuring integration of large-scale DEG arrays with large-scale microsupercapacitor (MSC) arrays (first-row images). The fabrication process diagram of MSC arrays (second-row images). Photograph of electrodes of (***i***) MSC arrays and (***ii***,***iv***) single MSC cells, and scanning electron microscope (SEM) images of the poly (3,4-ethylenedioxythiophene):poly(styrene sulfonate) (PEDOT:PSS)-based electrodes in (***iii***) top view and (***v***) cross-sectional view. Reproduced with permission from ref. [79]. Copyright 2025 Li et al. under the terms of a Creative Commons Attribution 4.0 International License, Springer Nature.

Power sources for small electronic components, low-power sensors, and wearable-compatible electronics are playing a growing role in the practical applications of D-TENGs and DEGs. Several studies now frame droplet generators as energy harvesters and practical micropower sources capable of charging capacitors, illuminating LEDs, or powering small electronic devices [71,76,80]. The device for harvesting multiple raindrops reported by Yang et al. [76] enables energy collection from multiple droplets, demonstrating its ability to charge a commercial calculator. Besides, Zhang et al. developed a direct-current device based on the dual-switch effect and EDL, enabling charging of a 1.5 V capacitor and powering a temperature and humidity sensor. This application direction is strengthened by device designs that improve charge extraction, prolong charge-transfer duration, or provide direct-current output, thereby reducing the mismatch between transient droplet signals and the requirements of downstream electronics [39,71].

D-TENGs and DEGs are increasingly being explored as self-powered sensing platforms. For sensing and monitoring acid rain and water pH levels, Min et al. [53] leveraged the hydrophobic and sticky properties of carnauba wax to fabricate a DEG. The device containing PDMS with 1 wt.% carnauba wax shows the greatest potential in monitoring water quality parameters, including temperature, pH, and heavy-metal ion concentrations. For wireless environmental sensing, Xu et al. [81] reported the DEG capable of enabling instantaneous self-powered wireless sensing from a single water droplet. Using a composite ferroelectric-triboelectric film, the device generates enough electricity to drive a real-time wireless sensing circuit with a 50 cm transmission range. Additionally, Wang et al. [67] developed a DEG using high-entropy ceramics as an intermediate layer that not only enables faster energy harvesting with an output voltage exceeding 500 V but also introduces a novel strategy for rapid bacterial detection. Furthermore, Liu et al. [82] developed a DEG capable of detecting DNA at the femtomolar level, whose intermediate layer is a high-dielectric composite of TiO_2, high-entropy sulfide, and PDMS (TiO_2/HES/PDMS). Several studies have shown that droplet-triggered electrical outputs can be engineered to encode environmental or biochemical information [53], enabling functions such as liquid-level monitoring [81], nitrate monitoring [83], and more [84]. Notably, the same droplet impact can serve simultaneously as a source of harvested energy and a carrier of analyte-relevant information, positioning droplet-based generators at the interface of energy harvesting and environmental intelligence.

A growing application area is their use in self-powered functional systems, where droplet-derived electrical signals are directly converted into visible or operational responses. Xu et al. [85] developed a raindrop-powered autonomous wireless hyetometer, showing the transition of D-TENGs from laboratory characterization to real-world deployment as a self-powered environmental monitoring system. The system integrates a raindrop-TENG array, energy-management module, signal-processing module, and wireless transmission module, in which the raindrop-TENG array simultaneously serves as an energy harvester and rainfall sensor; the harvesting units supply a regulated 2.5 V DC output, while the sensing units generate rainfall-dependent signals that are processed by a microprogrammed control unit and wirelessly transmitted over 10 m. With integrated design, it highlights the potential of droplet-TENGs for unattended weather monitoring, field surveys, IoT nodes, and early alerts for geological disasters. Similarly, Zhu et al. [86] merged a solid-liquid TENG with signal acquisition, data processing, and wireless transmission modules, enabling real-time droplet detection and rainfall estimation based on signal amplitude and frequency. With its high stability and analytical capability, the device is promising for roof rainwater monitoring, intravenous infusion monitoring, and automatic windshield wiper systems. Recently, Zhang et al. [87] revealed the integration of D-TENGs at the system level. They integrated a signal-processing and AI module with the device, using a deep fully connected neural network to analyze voltage and current outputs for classifying rainwater pH, demonstrating that D-TENGs can serve as both energy harvesters and self-powered sensors. In these systems, droplet energy is no longer treated as an isolated electrical output, but as a means of autonomous actuation, signaling, or environmental response. Despite the advancements, readiness for commercialization remains at the integrated-prototype phase. While notable instantaneous voltages and encouraging panel-scale outputs have been achieved, practical implementation is still hindered by inconsistent pulsed output, limited average usable power, inefficient storage solutions, array-level signal cancellation issues, environmental degradation, surface contamination, dielectric fatigue, and the need for long-term stability under actual rainfall conditions. As a result, it is more feasible to pursue near-term commercialization for battery-free sensors, warning systems, and hybrid building/environmental IoT platforms, whereas achieving grid-relevant energy production will necessitate standardized performance metrics, robust encapsulation, scalable manufacturing processes, and effective pulse-to-DC power management.

6. Outlook

The future direction for the development of D-TENGs and DEGs will focus on practical applicability rather than maximum output alone. The most promising avenues for advancement involve enhancing array-level scalability, exploring architectures that avoid rectifiers or employ direct current, creating device formats that are both mechanically durable and adaptable, and merging droplet-energy conversion with energy storage, wireless electronics, and self-powered sensing technologies. In this regard, the field's future prospects will likely be determined not by the maximum transient pulse generated by a single droplet but by efficiency, consistency, and intelligence with which numerous droplet events can be converted into usable electrical energy and practical information. The following are the challenges of droplet-energy technologies that should be addressed to evolve from conceptual demonstrations into reliable energy systems.

(i) Advancements in droplet-TENGs and DEGs necessitate progressing from merely describing individual mechanisms qualitatively to quantitatively identifying the interconnected dynamics of interfacial charge. Recent research has shed light on the roles of electron transfer, EDL evolution, electrostatic induction, redox chemistry, and contact-line electric fields; however, their relative contributions during real droplet impacts, sliding, evaporation, and various electrolyte conditions remain poorly understood. Future research should integrate real-time mapping of interfacial charges, time-resolved spectroscopy, controlled chemistry of electrolytes, and multiscale modeling to separate these influences. Gaining this mechanistic understanding will be crucial for developing devices that exhibit predictable polarity, enhanced charge retention, reduced breakdown, and consistent energy conversion.

(ii) High peak output does not necessarily translate into practically usable energy. Despite numerous devices indicating high instantaneous voltages, the energy collected is frequently delivered in brief, inconsistent pulses, resulting in constrained usable power output, inadequate current supply, and limited compatibility with storage electronics. Emerging evidence suggests that the primary constraint is not merely how much energy can be produced at once, but how briefly and unstably charge transfer occurs, highlighting the need to extend and stabilize this process for practical energy harvesting.

(iii) Efficiency decreases significantly during system scaling and integration. The efficiency of droplet-energy devices frequently declines significantly when moving from single-cell tests to practical arrays due to discrepancies in geometry between droplet dispersion and electrode configuration, highly intermittent output, and ineffective connection to energy storage systems. To successfully deploy large-scale systems, it is important to optimize the entire array and integrate microsupercapacitors or power-management circuits, instead of simply copying individual devices.

(iv) The devices lack sufficient durability when operating in realistic environmental conditions. Sustained deployment is still facing several challenges, including loss of charge, corrosion, dielectric fatigue, contamination, sensitivity to humidity, instability in wet conditions, and variations in water quality. Consequently, durability is becoming a key standard in the development of D-TENGs and DEGs, and using corrosion-resistant materials, managing interfaces, and designing for humidity tolerance are now recognized as essential for practical use, with their role extending beyond performance improvement.

(v) The applications of droplet-TENGs and DEGs should extend past individual demonstrations of powering LEDs to the development of integrated, information-enriched energy systems. Since each droplet event contains both mechanical energy and environmental data, these devices have significant potential for self-sustaining rainfall tracking, acid rain alerts, water quality monitoring, smart roofing, agricultural irrigation management, and decentralized environmental networks. The successful implementation of this technology will require stable integration of arrays, effective power-management circuits, corrosion-resistant materials, and reliable signal interpretation amid varying droplet sizes, frequencies, humidity levels, and water chemistry. Consequently, advancements focused on real-world applications should merge energy harvesting with sensing, data processing, and long-lasting durability.

(vi) In the emerging AI-driven era, AI-assisted strategies may help advance droplet-TENGs and DEGs from empirical optimization toward data-driven energy systems. In particular, AI-assisted optimization of droplet dynamics offers a promising direction for improving droplet-TENGs and DEGs beyond empirical trial-and-error design. By integrating high-speed imaging, electrical output mapping, and machine-learning analysis, concealed relationships between droplet size, impact speed, spreading area, contact duration, recoil behavior, surface wettability, and energy conversion efficiency can be discovered. Physics-informed models and closed-loop optimization have the potential to enhance the design of surface textures, dielectric layers, electrode shapes, and droplet-delivery conditions in order to optimize charge transfer while reducing rebound

loss, contact-line pinning, and parasitic capacitance. Such data-driven strategies may enable predictable, adaptive, and scalable droplet-energy systems under realistic rainfall and liquid-flow conditions.

In summary, the future of droplet-based energy harvesting will not rely on achieving higher instantaneous peak outputs but on the energy generated per droplet. Besides, it will depend on understanding how droplet-based energy harvesters work, delivering usable power effectively, creating devices that can be easily scaled, and ensuring long-term stability in operation. It is necessary to shift from focusing on improving individual outputs to developing the entire system to drive progress, guided by the physics of interfaces and metrics relevant to real-world applications. Addressing these issues in a coordinated way will be essential to establishing D-TENGs and DEGs as effective technologies for harvesting water energy.

Author Contributions

P.P.: investigation, formal analysis, data curation, writing—original draft, writing—review & editing; Y.Y.: conceptualization, supervision, funding acquisition, writing—review & editing. All authors have read and agreed to the published version of the manuscript.

Funding

This work was funded by the National Key R & D Project from the Ministry of Science and Technology in China (no. 2021YFA1201604).

Institutional Review Board Statement

Not applicable.

Informed Consent Statement

Not applicable.

Data Availability Statement

Data will be made available on request.

Conflicts of Interest

Given the role as Editor-in-Chief, Y.Y. had no involvement in the peer review of this paper and had no access to information regarding its peer-review process. Full responsibility for the editorial process of this paper was delegated to another editor of the journal.

Use of AI and AI-Assisted Technologies

No AI tools were utilized for this paper.

References

1. Mignon, V.; Saadaoui, J. How Do Political Tensions and Geopolitical Risks Impact Oil Prices? *Energy Econ.* **2024**, *129*, 107219. https://doi.org/10.1016/j.eneco.2023.107219.
2. REN21. Why Is Renewable Energy Important? Available online: https://www.ren21.net/why-is-renewable-energy-important/ (accessed on 24 March 2026).
3. Musie, W.; Gonfa, G. Fresh Water Resource, Scarcity, Water Salinity Challenges and Possible Remedies: A Review. *Heliyon* **2023**, *9*, e18685. https://doi.org/10.1016/j.heliyon.2023.e18685.
4. Hu, C.; Wang, Y.; Qi, L.; et al. Triboelectric Nanogenerators for Wave Energy Harvesting and Self-Powered Smart Sensing Applications. *Nano Energy* **2026**, *148*, 111657. https://doi.org/10.1016/j.nanoen.2025.111657.
5. Cheng, P.; Zou, Y.; Li, Z. Harvesting Water Energy through the Liquid–Solid Triboelectrification. *ACS Appl. Mater. Interfaces* **2024**, *16*, 47050–47074. https://doi.org/10.1021/acsami.4c09044.
6. He, T.; Wang, H.; Lu, B.; et al. Fully Printed Planar Moisture-Enabled Electric Generator Arrays for Scalable Function Integration. *Joule* **2023**, *7*, 935–951. https://doi.org/10.1016/j.joule.2023.04.007.
7. Wang, H.; Sun, Y.; He, T.; et al. Bilayer of Polyelectrolyte Films for Spontaneous Power Generation in Air up to an Integrated 1000 V Output. *Nat. Nanotechnol.* **2021**, *16*, 811–819. https://doi.org/10.1038/s41565-021-00903-6.
8. Lin, Z.-H.; Cheng, G.; Lee, S.; et al. Harvesting Water Drop Energy by a Sequential Contact-Electrification and Electrostatic-Induction Process. *Adv. Mater.* **2014**, *26*, 4690–4696. https://doi.org/10.1002/adma.201400373.

9. Hasan, M.A.M.; Zhang, T.; Wu, H.; et al. Water Droplet-Based Nanogenerators. *Adv. Energy Mater.* **2022**, *12*, 2201383. https://doi.org/10.1002/aenm.202201383.
10. Promsuwan, P.; Hasan, M.A.M.; Xu, S.; et al. Droplet Nanogenerators: Mechanisms, Performance, and Applications. *Mater. Today* **2024**, *80*, 497–528. https://doi.org/10.1016/j.mattod.2024.08.017.
11. Hu, Z.; Gong, S.; Chen, J.; et al. Energy Harvesting of Droplet-Based Triboelectric Nanogenerators: From Mechanisms toward Performance Optimizations. *DeCarbon* **2024**, *5*, 100053. https://doi.org/10.1016/j.decarb.2024.100053.
12. Wu, H.; Li, Y.; Wan, Q.; et al. From Liquid–Solid Contact Electrification to Triboelectric Nanogenerators: Mechanism, Methods and Applications. *Adv. Energy Mater.* **2026**, *16*, e05772. https://doi.org/10.1002/aenm.202505772.
13. Munirathinam, K.; Shanmugasundaram, A.; Lee, D.-W. Water-Based Triboelectric Nanogenerators: A Review. *Micro Nano Syst. Lett.* **2025**, *13*, 30. https://doi.org/10.1186/s40486-025-00252-2.
14. Freepik. Available online: www.freepik.com (accessed on 26 March 2026).
15. Chen, L.; Bonaccurso, E. Electrowetting—From Statics to Dynamics. *Adv. Colloid Interface Sci.* **2014**, *210*, 2–12. https://doi.org/10.1016/j.cis.2013.09.007.
16. Eid, K.F.; Panth, M.; Sommers, A.D. The Physics of Water Droplets on Surfaces: Exploring the Effects of Roughness and Surface Chemistry. *Eur. J. Phys.* **2018**, *39*, 025804. https://doi.org/10.1088/1361-6404/aa9cba.
17. Das, S.; Kumar, S.; Samal, S.K.; et al. A Review on Superhydrophobic Polymer Nanocoatings: Recent Development and Applications. *Ind. Eng. Chem. Res.* **2018**, *57*, 2727–2745. https://doi.org/10.1021/acs.iecr.7b04887.
18. Parvate, S.; Dixit, P.; Chattopadhyay, S. Superhydrophobic Surfaces: Insights from Theory and Experiment. *J. Phys. Chem. B* **2020**, *124*, 1323–1360. https://doi.org/10.1021/acs.jpcb.9b08567.
19. Antonini, C.; Villa, F.; Marengo, M. Oblique Impacts of Water Drops onto Hydrophobic and Superhydrophobic Surfaces: Outcomes, Timing, and Rebound Maps. *Exp. Fluids* **2014**, *55*, 1713. https://doi.org/10.1007/s00348-014-1713-9.
20. Srivastava, T.; Jena, S.K.; Kondaraju, S. Droplet Impact and Spreading on Inclined Surfaces. *Langmuir* **2021**, *37*, 13737–13745. https://doi.org/10.1021/acs.langmuir.1c02457.
21. Wang, Z.L. From Contact Electrification to Triboelectric Nanogenerators. *Rep. Prog. Phys.* **2021**, *84*, 096502. https://doi.org/10.1088/1361-6633/ac0a50.
22. Lin, S.; Xu, L.; Chi Wang, A.; et al. Quantifying Electron-Transfer in Liquid-Solid Contact Electrification and the Formation of Electric Double-Layer. *Nat. Commun.* **2020**, *11*, 399. https://doi.org/10.1038/s41467-019-14278-9.
23. Wu, J.; Cao, J.; Bi, H.; et al. Liquid-Solid Contact Electrification and Its Effect on the Formation of Electric Double Layer: An Atomic-Level Investigation. *Nano Energy* **2023**, *111*, 108442. https://doi.org/10.1016/j.nanoen.2023.108442.
24. Wang, Z.L.; Wang, A.C. On the Origin of Contact-Electrification. *Mater. Today* **2019**, *30*, 34–51. https://doi.org/10.1016/j.mattod.2019.05.016.
25. Lin, S.; Chen, X.; Wang, Z.L. Contact Electrification at the Liquid–Solid Interface. *Chem. Rev.* **2022**, *122*, 5209–5232. https://doi.org/10.1021/acs.chemrev.1c00176.
26. Wei, Y.; Li, X.; Gu, Y.; et al. Probing Electrical Double Layer via Triboelectric Charge Transfer. *Nat. Commun.* **2025**, *17*, 402. https://doi.org/10.1038/s41467-025-67094-9.
27. Jin, Y.; Yang, S.; Sun, M.; et al. How Liquids Charge the Superhydrophobic Surfaces. *Nat. Commun.* **2024**, *15*, 4762. https://doi.org/10.1038/s41467-024-49088-1.
28. Li, X.; Li, R.; Li, S.; et al. Triboiontronics with Temporal Control of Electrical Double Layer Formation. *Nat. Commun.* **2024**, *15*, 6182. https://doi.org/10.1038/s41467-024-50518-3.
29. Hu, Y.; Yang, W.; Ma, Y.; et al. Solid-Liquid Interface Charge Transfer for Generation of H_2O_2 and Energy. *Nat. Commun.* **2025**, *16*, 1692. https://doi.org/10.1038/s41467-025-57082-4.
30. Li, S.; Wang, Z.L.; Wei, D. Hidden Interfacial Electric Fields in Chemistry: Contact Electrification and Beyond. *Chem. Soc. Rev.* **2026**. *55*, 4756–4782. https://doi.org/10.1039/D5CS01066G.
31. Ye, C.; Liu, D.; Gao, Y.; et al. Electrostatic Breakdown at Liquid-Solid-Gas Triple-Phase Interfaces Owing to Contact Electrification. *Matter* **2025**, *8*, 102007. https://doi.org/10.1016/j.matt.2025.102007.
32. Yin, J.; Li, X.; Yu, J.; et al. Generating Electricity by Moving a Droplet of Ionic Liquid along Graphene. *Nat. Nanotechnol.* **2014**, *9*, 378–383. https://doi.org/10.1038/nnano.2014.56.
33. Zhang, Z.; Li, X.; Yin, J.; et al. Emerging Hydrovoltaic Technology. *Nat. Nanotechnol.* **2018**, *13*, 1109–1119. https://doi.org/10.1038/s41565-018-0228-6.
34. Lin, S.; Chen, X.; Wang, Z.L. The Tribovoltaic Effect and Electron Transfer at a Liquid-Semiconductor Interface. *Nano Energy* **2020**, *76*, 105070. https://doi.org/10.1016/j.nanoen.2020.105070.
35. Zheng, M.; Lin, S.; Tang, Z.; et al. Photovoltaic Effect and Tribovoltaic Effect at Liquid-Semiconductor Interface. *Nano Energy* **2021**, *83*, 105810. https://doi.org/10.1016/j.nanoen.2021.105810.
36. Li, Y.; Ren, H.; Hu, Z.; et al. Schottky MSM-Structured Tribovoltaic Nanogenerator Enabling over 25,000 nC Charge Transfer via Single Droplet Impact. *Adv. Mater.* **2025**, *37*, 2504902. https://doi.org/10.1002/adma.202504902.

37. Xu, W.; Zheng, H.; Liu, Y.; et al. A Droplet-Based Electricity Generator with High Instantaneous Power Density. *Nature* **2020**, *578*, 392–396. https://doi.org/10.1038/s41586-020-1985-6.
38. Riaud, A.; Wang, C.; Zhou, J.; et al. Hydrodynamic Constraints on the Energy Efficiency of Droplet Electricity Generators. *Microsyst. Nanoeng.* **2021**, *7*, 49. https://doi.org/10.1038/s41378-021-00269-8.
39. Dong, J.; Xu, C.; Zhu, L.; et al. A High Voltage Direct Current Droplet-Based Electricity Generator Inspired by Thunderbolts. *Nano Energy* **2021**, *90*, 106567. https://doi.org/10.1016/j.nanoen.2021.106567.
40. Hu, C.; Dan, H.; Zhu, W.; et al. Simultaneously Scavenging Multi-Type Energies via $BaTiO_3$ Film-Based Coupled Nanogenerator with High Coupling Factors. *Nano Energy* **2023**, *118*, 108976. https://doi.org/10.1016/j.nanoen.2023.108976.
41. Chen, Y.; Xie, B.; Long, J.; et al. Interfacial Laser-Induced Graphene Enabling High-Performance Liquid–Solid Triboelectric Nanogenerator. *Adv. Mater.* **2021**, *33*, 2104290. https://doi.org/10.1002/adma.202104290.
42. Meng, H.; Zhang, J.; Zhu, R.; et al. Elevating Outputs of Droplet Triboelectric Nanogenerator through Strategic Surface Molecular Engineering. *ACS Energy Lett.* **2024**, *9*, 2670–2676. https://doi.org/10.1021/acsenergylett.4c00532.
43. Zhang, J.; Zhou, Z.; Yang, X.; et al. Maximizing the Energy Scavenging Capability of Droplet Triboelectric Nanogenerators through Surface Engineering. *Nano Energy* **2024**, *127*, 109773. https://doi.org/10.1016/j.nanoen.2024.109773.
44. Liu, M.; Ding, X.; Xu, L.; et al. Dual Enhancement in Output Voltage and Energy of Droplet Electricity Generator via a Composite Dielectric Layer Design. *Small* **2025**, *21*, e07038. https://doi.org/10.1002/smll.202507038.
45. Li, Y.; Ma, G.; Zhu, L.; et al. From Interface Effect to Bulk Effect: Probing the Capacitive Coupling Enhancement Mechanism to Achieve High Performance DC Droplet-Based Nanogenerator. *Nano Energy* **2024**, *127*, 109743. https://doi.org/10.1016/j.nanoen.2024.109743.
46. Kuang, H.; Huang, S.; Zhang, K.; et al. Generating Direct Current Electricity from Ionic Droplets by Using Ferroelectric Material. *ACS Energy Lett.* **2023**, *8*, 3832–3838. https://doi.org/10.1021/acsenergylett.3c01381.
47. Li, S.; Zhang, Z.; Yang, F.; et al. Transistor-like Triboiontronics with Record-High Charge Density for Self-Powered Sensors and Neurologic Analogs. *Device* **2024**, *2*, 100332. https://doi.org/10.1016/j.device.2024.100332.
48. Wang, X.; Fang, S.; Tan, J.; et al. Dynamics for Droplet-Based Electricity Generators. *Nano Energy* **2021**, *80*, 105558. https://doi.org/10.1016/j.nanoen.2020.105558.
49. Dong, J.; Zhu, L.; Guo, P.; et al. A Bio-Inspired Total Current Nanogenerator. *Energy Environ. Sci.* **2023**, *16*, 1071–1081. https://doi.org/10.1039/D2EE02621J.
50. Li, Y.; Zhang, Q.; Cao, Y.; et al. A Constant-Current Generator via Water Droplets Driving Schottky Diodes without a Rectifying Circuit. *Energy Environ. Sci.* **2023**, *16*, 4620–4629. https://doi.org/10.1039/D3EE02280C.
51. Wang, J.; Cui, P.; Zhang, J.; et al. Boosted Energy Harvesting in Droplet Electrochemical Cell with Non-Equilibrium Electrical Double Layer. *Nano Energy* **2023**, *112*, 108437. https://doi.org/10.1016/j.nanoen.2023.108437.
52. Hu, C.; Wang, W.; Liu, Y.; et al. High-Output Solid-Liquid Triboelectric Nanogenerator Enhanced by the Regulation of Interfacial Wettability. *Nano Energy* **2024**, *130*, 110132. https://doi.org/10.1016/j.nanoen.2024.110132.
53. Min, G.; Wang, W.; Li, H.; et al. Optimizing Droplet-Based Electricity Generator via a Low Sticky Hydrophobic Droplet-Impacted Surface. *Small* **2024**, *20*, 2402765. https://doi.org/10.1002/smll.202402765.
54. Mai, V.-P.; Lee, T.-Y.; Yang, R.-J. Enhanced-Performance Droplet-Triboelectric Nanogenerators with Composite Polymer Films and Electrowetting-Assisted Charge Injection. *Energy* **2022**, *260*, 125173. https://doi.org/10.1016/j.energy.2022.125173.
55. Chen, X.; Zhang, Y.; Huang, Y.; et al. Interfacial Polarization-Enhanced Ultrahigh Performance Liquid Droplet Nanogenerator. *Adv. Energy Mater.* **2025**, *15*, 2406116. https://doi.org/10.1002/aenm.202406116.
56. Jang, S.; Lee, S.; Shah, S.A.; et al. Hydrogel-Based Droplet Electricity Generators: Intrinsically Stretchable and Transparent for Seamless Integration in Diverse Environments. *Adv. Funct. Mater.* **2025**, *35*, 2411350. https://doi.org/10.1002/adfm.202411350.
57. Luo, Q.; Ma, S.; Sun, W. GaN-Based Solid–Liquid Triboelectric Nanogenerator in Single-Electrode Mode. *ACS Appl. Electron. Mater.* **2026**, *8*, 501–509. https://doi.org/10.1021/acsaelm.5c02160.
58. Wang, H.L.; Zhang, B.; Chen, T.; et al. High-Efficiency Single-Droplet Energy Harvester for Self-Sustainable Environmental Intelligent Networks. *Adv. Energy Mater.* **2023**, *13*, 2302858. https://doi.org/10.1002/aenm.202302858.
59. Bao, C.; Zhang, M.; Liu, N.; et al. A Direct Current Droplet-Based Triboelectric Nanogenerator with a Suspended Probe and an Exposed Lower Electrode. *Nano Energy* **2025**, *145*, 111451. https://doi.org/10.1016/j.nanoen.2025.111451.
60. Lee, G.; Kim, E.; Choi, K.; et al. Droplet Electricity Generators with Maximized Energy Collection Zone Enabled by Aloe-Inspired Midrib and Cuticle. *Adv. Mater.* **2026**, *38*, e23637. https://doi.org/10.1002/adma.202523637.
61. Zhao, Z.; Li, H.; Li, A.; et al. Two-Orders of Magnitude Enhanced Droplet Energy Harvesting via Asymmetrical Droplet-Electrodes Coupling. *Nano Energy* **2023**, *108*, 108213. https://doi.org/10.1016/j.nanoen.2023.108213.

62. Wang, W.; Zhang, L.; Wang, H.; et al. High-Output Single-Electrode Droplet Triboelectric Nanogenerator Based on Asymmetrical Distribution Electrostatic Induction Enhancement. *Small* **2023**, *19*, 2301568. https://doi.org/10.1002/smll.202301568.
63. Meng, J.; Zhang, L.; Liu, H.; et al. A New Single-Electrode Generator for Water Droplet Energy Harvesting with a 3 mA Current Output. *Adv. Energy Mater.* **2024**, *14*, 2303298. https://doi.org/10.1002/aenm.202303298.
64. Prendergast, O.; Fatti, G.; Holmes, A.; et al. Taking Charge off Droplets: Introducing the Multi-Point Electrode TENG. *Chem. Eng. J.* **2025**, *525*, 170191. https://doi.org/10.1016/j.cej.2025.170191.
65. Wang, K.; Xu, W.; Li, J.; et al. Enhancing Water Droplet-Based Electricity Generator by Harnessing Multiple-Dielectric Layers Structure. *Nano Energy* **2023**, *111*, 108388. https://doi.org/10.1016/j.nanoen.2023.108388.
66. Ying, W.; Itoh, E. Improving the Performance of Water Droplet Power Generators by Inserting an Electron Trapping Layer into a Fluoropolymer Coated Polyimide Film. *Jpn. J. Appl. Phys.* **2025**, 64, 10SP25. https://doi.org/10.35848/1347-4065/ae08c0.
67. Wang, C.; Wang, J.; Wang, P.; et al. High-Entropy Ceramics Enhanced Droplet Electricity Generator for Energy Harvesting and Bacterial Detection. *Adv. Mater.* **2024**, *36*, 2400505. https://doi.org/10.1002/adma.202400505.
68. Shao, W.; Lin, T.; Liu, W.; et al. Field Enhanced Robust Droplet Electricity Generation. *Adv. Funct. Mater.* **2023**, *33*, 2302472. https://doi.org/10.1002/adfm.202302472.
69. Deng, Y.; Meng, G.; Tai, Y.; et al. Noncontact Liquid–Solid Nanogenerators as Self-Powered Droplet Sensors. *J. Mater. Sci. Mater. Electron.* **2023**, *34*, 1033. https://doi.org/10.1007/s10854-023-10389-8.
70. Yang, Y.; Lee, J.-H. Hybridized Nanogenerators: Materials and Structural Design for Improving Energy Harvesting. *MRS Bull.* **2025**, *50*, 416–427. https://doi.org/10.1557/s43577-025-00873-3.
71. Kam, D.; Gwon, G.; Jang, S.; et al. Advancing Energy Harvesting Efficiency from a Single Droplet: A Mechanically Guided 4D Printed Elastic Hybrid Droplet-Based Electricity Generator. *Adv. Mater.* **2023**, *35*, 2303681. https://doi.org/10.1002/adma.202303681.
72. Liu, D.; Yang, P.; Gao, Y.; et al. A Dual-Mode Triboelectric Nanogenerator for Efficiently Harvesting Droplet Energy. *Small* **2024**, *20*, 2400698. https://doi.org/10.1002/smll.202400698.
73. Zhang, Y.; Zhang, J.; Zheng, H.; et al. A Flexible Hybrid Generator for Efficient Dual Energy Conversion from Raindrops to Electricity. *Adv. Sci.* **2024**, *11*, 2404310. https://doi.org/10.1002/advs.202404310.
74. Xie, Y.; Zheng, J.; Guo, J.; et al. Triboelectricity-Enhanced Photovoltaic Effect in Hybrid Tandem Solar Cell under Rainy Condition. *Nano Energy* **2025**, *135*, 110647. https://doi.org/10.1016/j.nanoen.2025.110647.
75. Wang, S.; Wang, X.; Lu, C.; et al. Honeycomb Inspired Independent-Cell Droplet-Based Electricity Generator Array. *J. Bionic Eng.* **2024**, *21*, 2340–2348. https://doi.org/10.1007/s42235-024-00559-7.
76. Yang, Y.; Cao, B.; Yang, C.; et al. A Droplet-Based Multi-Position and Multi-Layered Triboelectric Nanogenerator for Large-Scale Raindrop Energy Harvesting. *AIP Adv.* **2023**, *13*, 055123. https://doi.org/10.1063/5.0148345.
77. Zheng, H.; Wu, H.; Yi, Z.; et al. Remote-Controlled Droplet Chains-Based Electricity Generators. *Adv. Energy Mater.* **2023**, *13*, 2203825. https://doi.org/10.1002/aenm.202203825.
78. Wu, X.; Cai, T.; Wu, Q.; et al. Droplet-Based Triboelectric Nanogenerators with Needle Electrodes for Efficient Water Energy Harvesting. *ACS Appl. Mater. Interfaces* **2025**, *17*, 13762–13772. https://doi.org/10.1021/acsami.4c17442.
79. Li, Z.; Chen, S.; Fu, Y.; et al. Efficiency Optimization for Large-Scale Droplet-Based Electricity Generator Arrays with Integrated Microsupercapacitor Arrays. *Nat. Commun.* **2025**, *16*, 8530. https://doi.org/10.1038/s41467-025-64289-y.
80. Pan, C.; Meng, J.; Jia, L.; et al. Droplet-Based Direct-Current Electricity Generation Induced by Dynamic Electric Double Layers. *ACS Appl. Mater. Interfaces* **2024**, *16*, 17649–17656. https://doi.org/10.1021/acsami.4c01168.
81. Xu, L.; Lu, J.; Coladas, G.J.; et al. Interfacial Engineering Enabled Single-Droplet Based Instantaneous Self-Powered Wireless Sensing. *Chem. Eng. J.* **2025**, *521*, 166940. https://doi.org/10.1016/j.cej.2025.166940.
82. Liu, Y.; Zhou, Y.; Wu, J.; et al. High-Performance Droplet Electricity Generator Biosensor for DNA Detection. *Cell Rep. Phys. Sci.* **2026**, *7*, 103091. https://doi.org/10.1016/j.xcrp.2025.103091.
83. Kaja, K.R.; Hajra, S.; Pharino, U.; et al. High-Performance Droplet-Driven Electrification for Self-Powered Real-Time Nitrate Monitoring in Agricultural Water Systems. *J. Sci. Adv. Mater. Devices* **2026**, *11*, 101154. https://doi.org/10.1016/j.jsamd.2026.101154.
84. Kaswan, K.; Ray, M.; Khan, A.; et al. Recent Advances in Solid-Liquid Triboelectric Nanogenerators for Self-Powered Chemical and Biological Sensing. *NPJ Biosensing* **2024**, *1*, 13. https://doi.org/10.1038/s44328-024-00011-0.
85. Xu, C.; Fu, X.; Li, C.; et al. Raindrop Energy-Powered Autonomous Wireless Hyetometer Based on Liquid–Solid Contact Electrification. *Microsyst. Nanoeng.* **2022**, *8*, 30. https://doi.org/10.1038/s41378-022-00362-6.
86. Zhu, L.; Guo, L.; Ding, Z.; et al. Self-Powered Intelligent Water Droplet Monitoring Sensor Based on Solid–Liquid Triboelectric Nanogenerator. *Sensors* **2024**, *24*, 1761. https://doi.org/10.3390/s24061761.
87. Zhang, Z.; Wang, J.; Liu, Y. Enhanced Droplet Triboelectric Nanogenerator via Interfacial Engineering for Raindrop Energy Harvesting and pH Monitoring. *Langmuir* **2026**, *42*, 9239–9247. https://doi.org/10.1021/acs.langmuir.5c06538.